Int. J. Electrochem. Sci., 8 **(2013)** 2204 - 2219

International Journal of
ELECTROCHEMICAL
SCIENCE
www.electrochemsci.org

Anodic Performance of Mesoporous TiO_2-C Composites with Cu Nanopaticles Embedded for Lithium Ion Battery

Song Gyun Lee, Honggui Deng, Jun Hu[*]*, Lihui Zhou, Honglai Liu*

State Key Laboratory of Chemical Engineering and Department of Chemistry, East China University of Science and Technology, 130 Meilong Road, Shanghai 200237, China
[*]E-mail: junhu@ecust.edu.cn

Received: 14 December 2012 / *Accepted:* 5 January 2013 / *Published:* 1 February 2013

Ordered mesoporous TiO_2-C composites with Cu nanoparticles embedded (TiO_2-C-Cu) have been prepared *via* an evaporation induced of self-assembly (EISA). Through controlling the hydrolysis of Ti species by the acid-base pair of $TiCl_4$ and $Ti(OBu)_4$ precursors, the ordered mesoporous structure with a large surface area of 161.9 $m^2 g^{-1}$ are obtained. The structure-directing of polymer Pluronic P123 are convert into a sturdy carbon and metallic Cu nanoparticles are highly dispersed in the mesoporous TiO_2-C composites after the calcinations in a N_2 flow. When the composites are used as the anode material for lithium ion batteries, the lithium storage performance are effectively improved by "Cu-embedded" nanoparticles at low current density. The reversible capacity of TiO_2-C-Cu could be stable at 150.0 mAh g^{-1} when the current density is 33.4 mA g^{-1}. Moreover, the electrochemical impedance spectroscopy (EIS) and cycle voltammogram (CV) analysis further reveal that the electrochemical performance of TiO_2-C-Cu composite is significantly improved by "Cu-embedded", as well as by the ordered mesoporous channels. Accordingly, metal-embedded in mesoporous TiO_2-C composites would be a promising way to improve the electrochemical performance of TiO_2 as the anode material in lithium ion battery.

Keywords: Lithium ion battery; Anode material; TiO_2 nanocomposite; Cu-embedded; Electrochemical performance

1. INTRODUCTION

Lithium ion batteries have been widely applied to various fields ranging from small electronic devices to electric vehicles. Many efforts have been devoted to the electrode materials that provide high energy storage capacity, fast charge rate, long duration, as well as low production cost. TiO_2, as one of the most promising anode materials, has attracted much attention because of its superior characteristics [1, 2]. The characteristic of "zero-strain" makes TiO_2 not suffering from the structural

deformation during electrochemical process; furthermore, the lithium insertion voltage in TiO_2 is 1.5 V (*vs*. Li/Li^+), much higher than the Li electroplating potential, so the solid electrolyte interface (SEI) will unlikely form. However, the low electrical conductivity of TiO_2 results in a sluggish electrode kinetic of lithium ion insertion/extraction especially at high charge/discharge rate. One strategy to solve this problem is to fabricate TiO_2 into nanoscale materials, such as nanospheres, nanotubes, and nanowires which can effectively decrease the diffusion distance for lithium ions [3-5]. However, the intrinsic aggregation of TiO_2 nanoparticles inevitably causes decreases of the electrochemical property with time. To keep TiO_2 nanoparticles from aggregating, TiO_2-based mesoporous materials have been proposed, in which the cylinder mesoporous channel would be a facilitated path for Li^+ ion transfer; and small TiO_2 grains in the matrix would effectively reduce the diffusion length for Li^+ ion insertion/extraction [6-11].

The mesoporous materials were usually synthesized by using hard or soft template [12-15]. The key point for the successful synthesis of mesoporous materials is that the hydrolysis and condensation rates should be precisely controlled throughout the process [16]. However, the hydrolysis of most titanium precursors, such as $TiCl_4$, $Ti(OPr)_4$, $Ti(Obu)_4$, proceeds too quickly to obtain the ordered meso-TiO_2 *via* common hydrothemal methods. One strategy is to change the self-assembly method. It has been approved that evaporation induced of self-assembly (EISA) method with the soft template existing, developed by Briker et al. [17] would be a good way to fabricate the ordered mesoporous TiO_2. Another strategy is to find the suitable titanium precursors. Tian et al. [18] proposed an acid-base pair precursor strategy to self-control the rate of hydrolysis of titanium precursors to obtain the desired mesostructure. More importantly, during the calcination, the fast growth of TiO_2 nanocrystals usually results in the pore shrinkage, or even worse, the collapse of the mesostructure. The coexisting carbon species in mesoporous TiO_2 has been approved as an effective way to prevent the excessive growth of TiO_2 nanocrystals, and hence improves the thermal stability of the mesostructure. Tang et al. [19] reported that mesoporous TiO_2 with highly crystallized structure can be stabilized by the amorphous carbon through careful calcination. Recently, Liu et al. [20] reported that highly ordered mesoporous carbon-titania nanocomposites with nanocrystal-glass "bricked-mortar" frameworks were synthesized *via* the organic-inorganic-amphiphilic coassembly. Lee et al. [21] synthesized mesoporous TiO_2-Carbon-Nb_2O_5 nanocomposite *via* a one-pot process using the block copolymer as a structure-directing agent which converted into a sturdy carbon. In fact, the carbon skeleton not only played the role as "mortar" to hold the mesoporous structure of TiO_2, but also can improve its poor conductivity [22, 23]. However, the carbon content in composites should be carefully control, since the lithium insertion voltage in carbon negative electrode (0.01 V *vs*. Li/Li^+) would easily induce the formation of the SEI film and resulted in a poor electrochemical performance. Besides carbon, metal-embedded in the matrix of TiO_2 could be another economic and promising way to improve its conductivity. Guo et al. [24] reported the superior electrode performance of mesoporous TiO_2 mixed with RuO_2 nanoparticles, the specific charge capacity could maintained as large as 91.0 mAh g^{-1} at very high rate of 5.0 A g^{-1}.

However, to our knowledge, there are very few attempts to mixed carbon and metal together into mesoporous TiO_2 to improve its electrochemical properties. In this paper, the ordered mesoporous nanocomposites of TiO_2 containing carbon and Cu nanoparticles were synthesized through the EISA method and *in-situ* crystallization. TiO_2-C-Cu and TiO_2-C composites were comprehensively

investigated to make a fundamental understanding between the structure and the electrochemical performance. The lithium storage performance of TiO_2-C-Cu can be significantly improved by "Cu-embedded", as well as by the existence of the ordered mesoporous structure. Accordingly, TiO_2-C-Cu composites showed promising lithium insertion/extraction characteristics as an anode material for lithium ion battery.

2. EXPERIMENTAL PART

2.1 Materials

Triblock poly(ethylene oxide)-*b*-poly(propylene oxide)-*b*-poly(ethylene oxide) copolymers Pluronic P123 ($EO_{20}PO_{70}EO_{20}$, M_{av} = 5,800) was purchased from Sigma–Aldrich Corp. Titanium tetrachloride ($TiCl_4$), Tetrabutyl titanate ($Ti(OBu)_4$), $Cu(CH_3COO)_2$, phenol, formalin aqueous solution (37 wt%), NaOH, and ethanol were purchased from Shanghai Lingfeng Chemical Reagent Corp. All chemicals were analytical grade and used directly without further purification.

2.2 Synthesis

Before the synthesis of TiO_2 mesoporous composites, the resol polymer was synthesized according the method described elsewhere [25]. The EISA method followed by *in-situ* crystallization was adopted to prepare TiO_2-C and TiO_2-C-Cu mesoporous composites. In a typical synthesis, the acid-base pair precursor (0.85 g of $TiCl_4$ and 1.5 g of $Ti(OBu)_4$), 20 wt% resol ethanol solution (1 g), and ethanol solution (12.0 mL, containing 1.0 g of P123 and 0.1 g of $Cu(CH_3COO)_2$) were mixed together under vigorous stirring at 0 °C. After stirring for 5 min, the red sol-solution was poured into a Petri dish, and transferred into a 35 °C oven. A transparent membrane was produced after the evaporation for 48 h. Then, it was undergone a heat-treatment at 100 °C for 24 h to obtain the as–synthesized TiO_2-C-Cu. Finally, the membrane was scraped from the dish for the calcination. The calcination was carried out in a tubular furnace under nitrogen gas protecting, with a heating rate of 0.5 °C min^{-1}. After holding at 350 °C for 2 h, the sample of TiO_2-C-Cu-350 was obtained, and then the temperature further increased to 500 °C, after 2 h, the obtained sample was denoted as TiO_2-C-Cu-500.

For comparison, the ordered mesoporous TiO_2-C samples were synthesized in the same way but without adding $Cu(CH_3COO)_2$. The obtained samples were denoted as TiO_2-C-350 and TiO_2-C-500, respectively, depending on the calcination temperature.

2.3 Characterization

The X-ray powder diffraction (XRD) data were collected on a Rigaku D/max 2550 VB/PC diffractometer with Cu Kα X-radiation at 40 kV and 50 mA. High-resolution transmission electron microscopy (HRTEM) were carried out on a JEOL JEM-2010 microscope. Samples were prepared by dispersing particles in ethanol first under the ultrasonification and then dropping the suspension on a

copper grid doped with a holey carbon film. Nitrogen adsorption–desorption isotherms were determined on an ASAP-2020 analyzer at -196 °C. Prior to the measurement, the samples were first degassed at 100 °C under vacuum for at least 6 h. The surface areas were calculated by the Brunauer–Emmett–Teller (BET) method. The pore size distributions were derived from the desorption branches of the isotherms using the Barrett–Joyner–Halenda (BJH) model. Thermogravimetric analysis (TGA) was carried out on a NETZSCH STA 499F3 thermal analyzer. The heating rate is 5 °C min^{-1} and the flow gas is nitrogen or mixed gases of nitrogen (80 %) and oxygen (20 %) with a flow rate of 100 mL min^{-1}. X-ray photoelectron spectroscopy (XPS) analysis was carried out on a Kratos Axis Ultra DLD spectrometer.

2.4 Electrochemical characterization

The working electrode was prepared from a mixture of sample powders, carbon black conducting agent and polyvinylidene fluoride (PVDF) binder, with a weight ratio of 70:15:15 in n-methyl-2-pyrrolidinone (NMP) solvents, The slurry was pasted on a copper foil. Electrochemical test cells were assembled in an argon-filled glove box, using coin-type half-cells with lithium foil as a counter electrode. The electrolyte was 1.0 M $LiPF_6$ in a mixture of ethylene carbonate (EC) and dimethyl carbonate (DMC) (1:1 v/v). The cells were galvanostatically charged and discharged in a voltage range from 1.0 to 3.0 V *vs.* Li/Li^+. The rate performance was measured at the current densities varying from 0.2 C (33.40 mA g^{-1}) to 20 C (3340 mA g^{-1}). The cycle performance for 100 cycles was recorded at the current density of 0.5 C. Cyclic voltammogram (CV) tests were conducted on a Gamry Instrument at a scan rate of 0.1 mV s^{-1} in the voltage range of 1.0 - 3.0 V. All the electrochemical measurements were carried out at room temperature on an Arbin BT2000 battery test system.

3. RESULTS AND DISCUSSIONS

3.1 Structures of mesoporous TiO_2 composites

By using acid-base ($TiCl_4$ - $Ti(OBu)_4$) pair titanium precursors *via* a modified EISA method, the hybrid mesoporous composite membranes of TiO_2-C and TiO_2-C-Cu were synthesized. All the as-synthesized composite membranes were transparent and homogenous, without macro-phase separation. The ordered mesoporous structures were evidenced by XRD patterns in the small-angle range (SAXRD). As shown in Figs. 1a and 1c, each pattern (1) of as-synthesized TiO_2-C and TiO_2-C-Cu shows a week diffraction peak at $2\theta \sim 1$ º, suggesting the existence of mesopores. After the calcination in a N_2 flow at 350 °C, the products were black-colored. Each pattern (2) of TiO_2-C-350 and TiO_2-C-Cu-350 shifts to a larger angle diffractions of $2\theta = 1.266$ º and 1.278 º, respectively. Enlarging each pattern (2) by 3 times, each pattern (4) shows more weak diffraction peaks, which can be approximately indexed as (10), (11) and (20) planes of 2D hexagonal *P6mm* symmetry [26]. The intensities of both composite patterns significantly increase, revealing structures become more ordered after proper calcination. Although the diffraction of (10) plane of TiO_2-C-Cu becomes broad, but no

significant change of 2θ position is observed, and the corresponding *d*-spaces of (10) plane of TiO_2-C-350 and TiO_2-C-Cu-350 are about 6.9 nm, suggesting "Cu-embedded" had little effect on the mesoporous lattices. Without adding resol polymer, the ordered mesoporous structure was collapsed even at 350 °C，implying that the existence of carbon can stabilize the mesoporous structure of TiO_2 to a certain extent, With the calcination temperature further increasing to 500 °C, the (10) diffraction peak in each pattern (3) becomes less-resolved, and the original weak (11) and (20) peaks completely disappear, indicating the degradation of the ordered structure. So when the carbon content was less than 30 %, no significant stabilization effect of carbon can be detected at 500 °C, and the growth of crystalline TiO_2 in the wall was the main reason for the collapse of the ordered mesoporous structure.

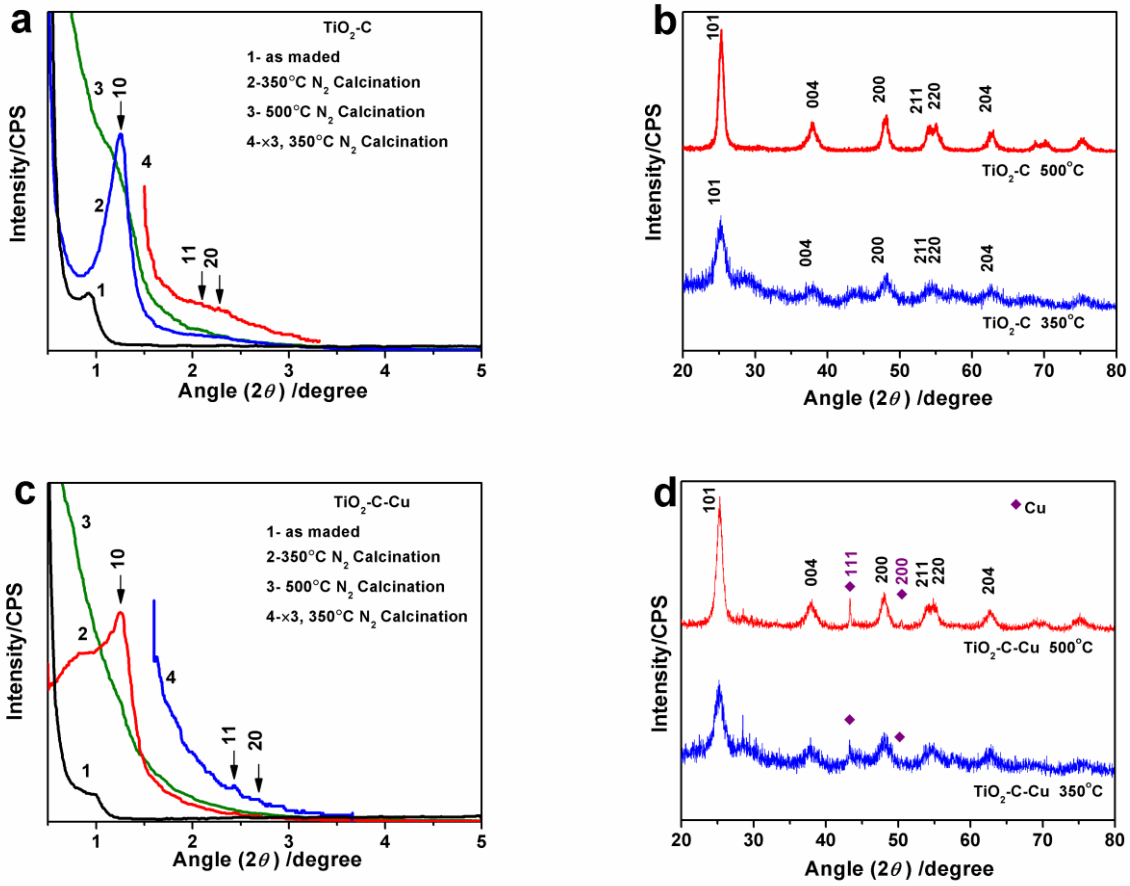

Figure 1. SAXRD and WAXRD patterns of the hybrid mesoporous composites before and after calcination at different temperatures of 350 and 500 °C; **a, b** TiO_2-C, and **c, d** TiO_2-C-Cu.

Wide-angle XRD (WAXRD) further revealed the changes of the crystal structure of the composites with the calcination temperature. Figs. 1b and 1d are the WAXRD patterns of TiO_2-C and TiO_2-C-Cu calcinated under N_2 protecting at 350 and 500 ^oC, respectively. The diffraction intensities of crystalline TiO_2 for both composites increase with the calcination temperature. Although the composites calcinated at 350 ^oC contained some portions of the amorphous phase, (101), (004), (200), (211), (220) and (204) diffractions of typical anatase TiO_2 (JCPDS: 21-1272) can be still detected.

When the calcination temperature increased to 500 ^{o}C, six major peaks are distinct which can be assigned to the typical anatase TiO_2 without any other polymorph coexisted. Estimated from the space value of the (101) lattice plane of anatase by Debye-Scherrer equation (D=0.89λ/βcos(θ)), the average size of TiO_2-C-Cu-350 crystals is about 3 nm, and it grows up to 8~9 nm at the calcination temperature of 500 °C. The presence of Cu is significantly evidenced by WAXRD patterns of TiO_2-C-Cu, being consistent with the diffraction peaks of (111), (200) of Cu standard pattern (JCPDS: 04-0836) [27]. It indicates that copper oxide would be reduced to Cu metal by some reductant like carbon monooxide generated by decomposition of resol polymer or surfactant template during the calcination process with a N_2 flow protection.

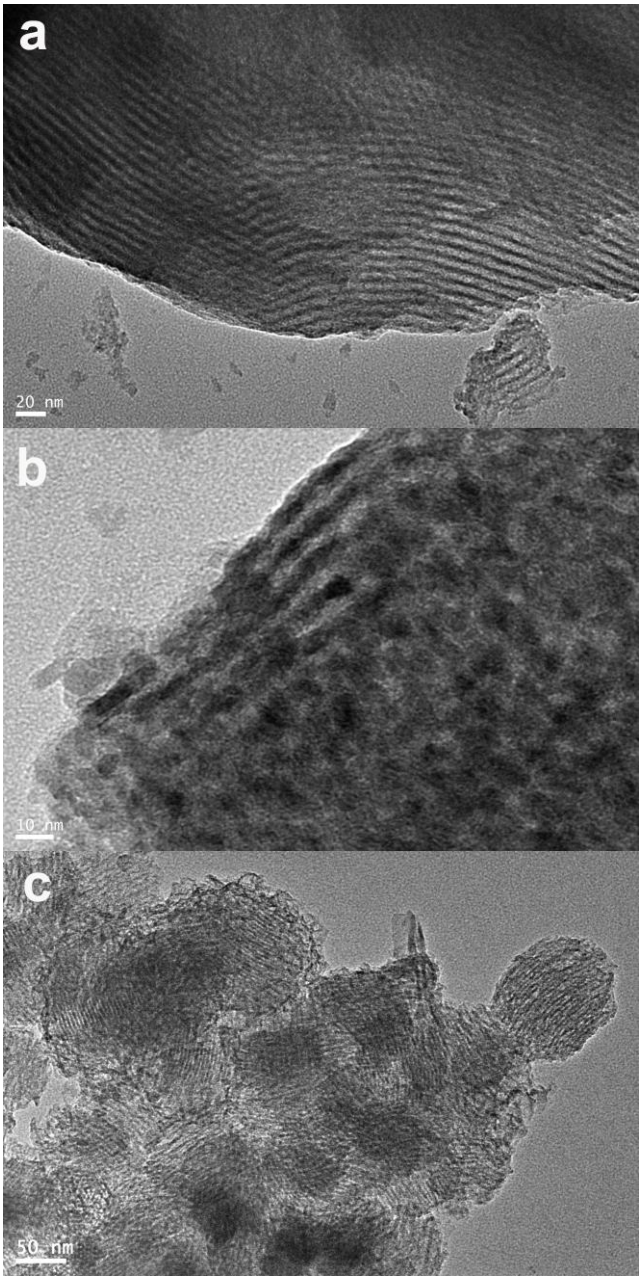

Figure 2. TEM images of composites calcined at 350 °C in a N_2 flow; **a** TiO_2-C, and **b, c** TiO_2-C-Cu.

Transmission electron microscope (TEM) images in Fig. 2 show that both TiO_2-C-350 and TiO_2-C-Cu-350 composites possess ordered mesoporous structures, being consistent with SAXRD results (Figs. 1a and 1c). The average diameters of the channels of both composites are about 5.0 nm. No separated phases of carbon can be observed, suggesting TiO_2 and resol polymer are well-mixed during the EISA process. Fig. 2b shows that Cu nanoparticles are highly dispersed in the wall of the mesoporus composite. Fig. 2c further reveals that TiO_2-C-Cu-350 composite consists of spherical mesoporous particles with an average size of 200~300 nm.

The evidence of the chemical states of Cu in TiO_2-C-Cu at 350 and 500 ^oC were further illustrated by XPS. As shown in Fig. 3a, Cu 2p binding energies in the XPS spectra of TiO_2-C-Cu-350 shows two peaks at 932.2 eV and 933.5 eV, which are attributed to Cu-Cu (metal) and Cu-O, respectively. The peak at 932.2 eV is dominant, indicating metallic Cu nanopaticles are embedded in TiO_2-C-Cu at 350 ^oC, only small amount of CuO are formed. With increasing the calcination temperature, as shown in Fig. 3b, besides the original two peaks, there is a new peak at 935.0 eV dominated in the XPS spectra of TiO_2-C-Cu-500, which is attributed to Cu-Cl. Since we used $TiCl_4$ as Ti precursor, Cu-Cl bounding would be easily formed at high calcination temperature in N_2 atmosphere.

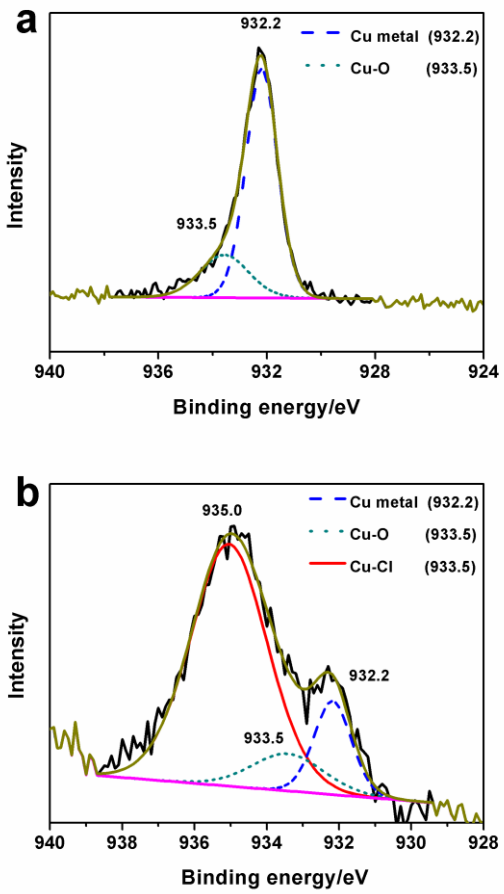

Figure 3. XPS Cu 2p Bonding energy images of TiO_2-C-Cu composite calcined in a N_2 flow at different temperatures **a** of 350, and **b** of 500 °C.

The mass ratio of TiO_2 and carbon in the hybrid composites can be estimated by the thermogravimetric analysis (TGA). As shown in Fig. 4, when the as-synthesized TiO_2-C-Cu sample is heated from the room temperature to 800 °C in a N_2 flow, the TG curve exhibits two-step mass loss levels. The first level, below 200 °C, shows a mass loss of about 10 %, attributed to the evaporation of water and the solvent. The second level, 200 - 350 °C, has a mass loss of about 54 %, related with the decomposition and transformation of triblock template P123 and some resol into carbon. After 350 °C, the sample shows a little mass loss, suggesting that a small part of highly cross-linked resol networks may be still preserved in TiO_2-C-Cu-350. When 20 % (v/v) O_2 was added into N_2 flow, for the same sample, it shows a mass loss of 64 % in the range of 200-500 °C due to the completely burning off of resol and triblock copolymers. Compared with the mass loss of 54 % in a N_2 flow, it can be estimated that the carbon amount is about 9.0 % in the as-synthesized sample, namely, about 25 % in the product of TiO_2-C-Cu after calcination. Based on analysis data, the total amount of TiO_2 and Cu was about 27 % in as-synthesized sample, namely about 75 % in the product of TiO_2-C-Cu. The insert in Fig. 4 is the DSC curve of TiO_2-C-Cu sample in a N_2 flow. The peak emerged at 200 °C in the DSC curve may be attributed to the enhanced polymerization of resol. The result is consistent with the evidence that the cross-cracking of carbon framework occurred and the "soft" framework transformed to a relatively "rigid" one in the range of 200-500 °C [28, 29]. However, the heat of the exothermic reduction of Cu is too small to be observed. Based on TGA and XPS elemental analysis, it was found that the weight ratio of each components was 70 TiO_2:25 Carbon:5 Cu and 70 TiO_2:30 Carbon for TiO_2-C-Cu and TiO_2-C, respectively.

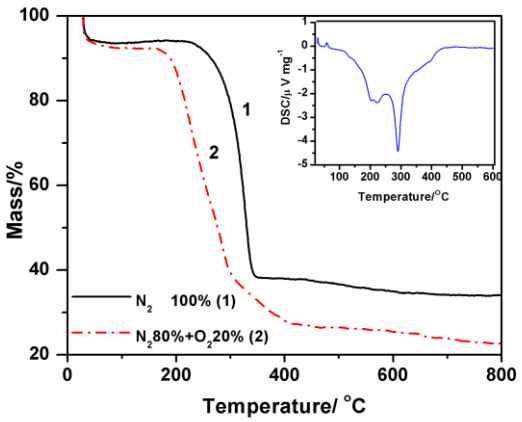

Figure 4. TG curves of as-synthesized TiO_2-C-Cu in different gas flow conditions of N_2 and N_2 80 %+O_2 20 % with the heating rate of 5 °C min^{-1}. In the *inset*: DSC curve of as-synthesized TiO_2-C-Cu in a N_2 gas flow.

Fig. 5 shows N_2 adsorption/desorption isotherms of TiO_2-C-Cu. The isotherms are a typical IV type with a hysteresis cycle, in which the onsets of the capillary condensation are at P/P^o of 0.55 for TiO_2-C-Cu-350 and 0.65 for TiO_2-C-Cu-500, respectively. The desorption hysteresis of TiO_2-C-Cu-500 starts at the P/P^o of 1, suggesting the existence of some packing pores due to the growth of TiO_2

nanoparticles. The insert of Fig. 5 shows that TiO_2-C-Cu-350 has a relatively narrow pore distribution at about 5.9 nm; whereas TiO_2-C-Cu-500 shows a broadened pore distribution, and it shifts to larger average pore size of 10.5 nm. Moreover, the BET surface area decreases from 161.9 $m^2 g^{-1}$ of TiO_2-C-Cu-350 to 91.4 $m^2 g^{-1}$ of TiO_2-C-Cu-500, suggesting some mesoporous structure of TiO_2-C-Cu collapsed with increasing the calcination temperature. Calculated through N_2 adsorption/desorption isotherms, XRD patterns, and TEM images, Table 1 lists the comparison results of structural properties of TiO_2-C-350 and TiO_2-C-Cu-350. After the calcination at 350 ^oC in a N_2 flow, the structural properties are similarly compared with each other, such as unit cell parameters of 8.04 and 7.97 nm, thickness of porous walls of 2.91, 2.92 nm, and sizes of TiO_2 crystal of 2.75 and 2.80 nm for TiO_2-C-350 and TiO_2-C-Cu-350, respectively, suggesting that "Cu-embedded" had little effect on the structure properties of the composites.

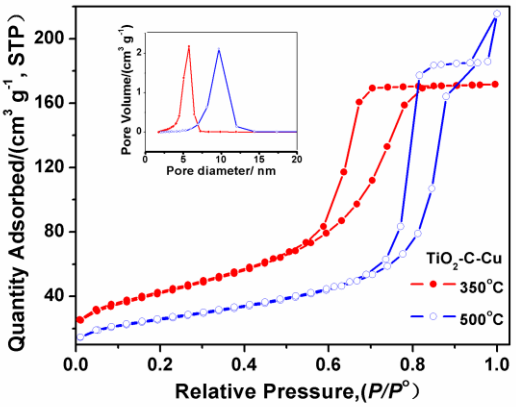

Figure 5. Nitrogen adsorption/desorption isotherms of TiO_2-C-Cu calcinated at 350 °C and 500 °C in a N_2 gas flow. In the *inset*: pore diameter distributions.

Table 1. Structural properties of TiO_2-C and TiO_2-C-Cu after the calcination at 350 ^oC in a N_2 gas flow.

Sample	d_{10}[a] (nm)	a_0[b](nm)	D_P[c](nm)	W_t[d] (nm)	D[e](nm)	S_{BET} ($m^2 g^{-1}$)	V_P ($cm^3 g^{-1}$)
TiO_2-C	6.97	8.04	5.13	2.91	2.75	144.4	0.25
TiO_2-C-Cu	6.91	7.97	5.05	2.92	2.80	161.9	0.23

where [a]d_{10}, interplanar distance of (10) plane, determined from (10) peaks of SAXRD; [b]a_0, unit-cell parameter, calculated by $a_0=2d_{10}/3^{1/2}$; [c]D_P, Pore diameter, calculated by the BJH method from N_2 desorption isotherm; [d]W_t, thickness of the wall, calculated by $W_t=a_0-D_P$; [e]D, nano-crystal size, calculated by Scherrer formula ($(D=0.89\lambda/\beta\cos(\theta))$, where β (unit, rad) is the full-width at half-maximum of the (101) diffraction peek for anatase TiO_2, λ is the wavelength of Cu Kα-irradiation

source (0.15406 nm), θ (unit, degree) is the angle of the diffraction peak, and 1 rad=180°/π ≈57.2958° [28].

3.2 Electrochemical properties

The effect of "Cu-embedded" on the anodic behavior for lithium ion batteries was further investigated by comparing the electrochemical properties of the composites of TiO_2-C and TiO_2-C-Cu after the calcinated at 350 °C in a N_2 gas flow. The Li^+ insertion/extraction reaction in TiO_2 can be expressed as Eq. 1;

$$TiO_2 + xLi^+ + xe^- \rightarrow Li_xTiO_2 \quad (1)$$

where x is the insertion coefficient, usually close to 0.5 for anatase crystal [2]. Theoretical electrochemical capacity of $Li_{0.5}TiO_2$ is 167 mAh g^{-1} corresponding to the current density of 1 C h, where 1 C is 167 mA g^{-1}.

Fig. 6 shows galvanostatic charge/discharge profiles of TiO_2-C and TiO_2-C-Cu composites at 1, 5, 100th cycle, and the current density is 0.5 C. As shown in Fig. 6a, the first discharge capacity of TiO_2-C is 178.8 mAh g^{-1}, while the charge is 108.5 mAh g^{-1}, corresponding to a coulombic efficiency of 60.7 %. However, the discharge/charge capacity of the first cycle for TiO_2-C-Cu, as shown in Fig. 6b, is 193.8/165.0 mAh g^{-1}, respectively, and the corresponding coulombic efficiency is 85.1 %, which is higher than that of TiO_2-C. The first cyclic discharge curves of both composites reveal a small 'hysteresis' at about 1.2 V by some defects in the anatase framework [30], and thereafter it disappears after 10 cycles. The charge/discharge potential plateaus of TiO_2-C-Cu and TiO_2-C are at 2.1 and 1.7 V, respectively. Compared with TiO_2-C, TiO_2-C-Cu has a much longer plateau suggesting the "Cu-embedded" has a positively effect on faster electron conducting in three-dimensional network in TiO_2-C-Cu composite.

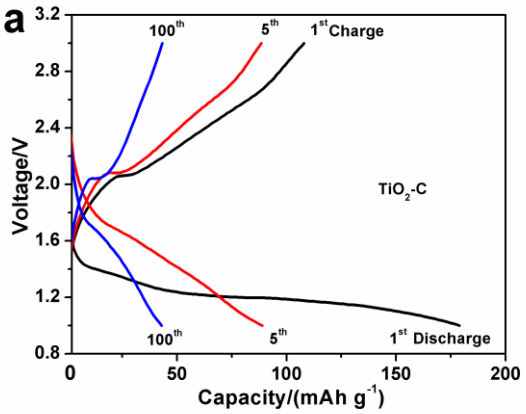

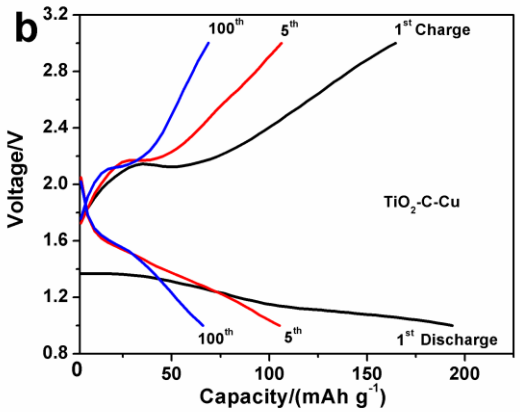

Figure 6. Galvanostatic charge (Li extraction)/discharge (Li insertion) profiles obtained from different composites during 1, 5, 100th cycle at the current density of 0.5C; **a** TiO_2-C, and **b** TiO_2- C-Cu.

Fig. 7 shows the cycle performance of TiO_2-C and TiO_2-C-Cu at 0.5 C. The capacity for both composites drops quickly during the first 15 cycles, and thereafter it stabilizes at an almost constant value even up to 100 cycles without noticeable capacity fading. For TiO_2-C-Cu composite, the stable discharge is 75 mAh g^{-1}, with a small capacity fading of 10 % relative to the 15th cycle capacity. Meanwhile, the capacity of TiO_2-C decays much quicker than that of TiO_2-C-Cu after the 15th cycle, and its stabile capacity is 50 mAh g^{-1}. It implies that Cu nanoparticles embedded in the composites may play a significant role for improving conductivity, which results in the improvement of diffusion of Li^+, and the high columbic efficiency, as well.

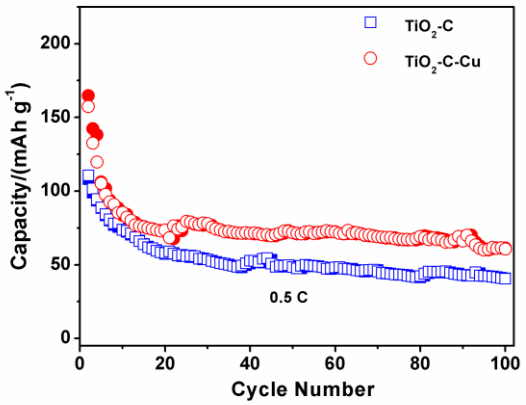

Figure 7. Cycling performance at 0.5 C of TiO_2-C and TiO_2-C-Cu composites.

Fig. 8 displays the high rate performance of TiO_2-C and TiO_2-C-Cu at different current densities in the potential range of 1.0 - 3.0 V. The reversible capacities of both composites rapidly decrease at current density of 0.2-0.5 C, followed by a gradual decrease with further increasing current density to1-20 C. The reversible capacities of TiO_2-C are about 105, 50, 30, 28, 20, 20, and 20 mAh g^{-1}

at different current densities of 0.2, 0.5, 1, 2, 5, 10, and 20 C, respectively, higher than that of commercial titania reported by Baudrin et al. [31]. It reveals that the improved characteristics, such as the ordered mesoporous architecture, the high specific surface area, and the existence of carbon in TiO_2-C composites, facilitate the transfer of lithium ions. Meanwhile, TiO_2-C-Cu composite has even higher rate performance, with the reversible capacities of 150, 75, 35, 28, 25, 20, and 20 mAh g^{-1} at different current densities as mentioned above, respectively. At low current density range of 0.2-0.5 C, TiO_2-C-Cu shows much larger capacity than that of TiO_2-C, whereas, at high current density range of 2-20 C, there is no obvious difference in capacity. It reveals that the effect of "Cu-embedded" on the capacity is significant at low current density, which may be attributed to the decrease of activation energy necessary for charge transfer; whereas, at high current density range, the inhibition of mass-transfer is dominated rather than the improvement of charge transfer mentioned above, which results in the similar limiting capacity for both composites. In addition, when the current rate is again reduced back to 0.2 C, the reversible capacity can be recovered and maintains at 125 mAh g^{-1}, which is larger than 80 mAh g^{-1} of TiO_2-C, indicating TiO_2-C-Cu with "Cu-embedded" is a quite good anode material. Compared with the results of mixing RuO_2 [24] to improve the conductivity of TiO_2, although the capacity performance of TiO_2-C-Cu composite was a little lower that of TiO_2-RuO_2, Cu is a promising agent with good conductivity, much cheaper, and easily manageable to the industry.

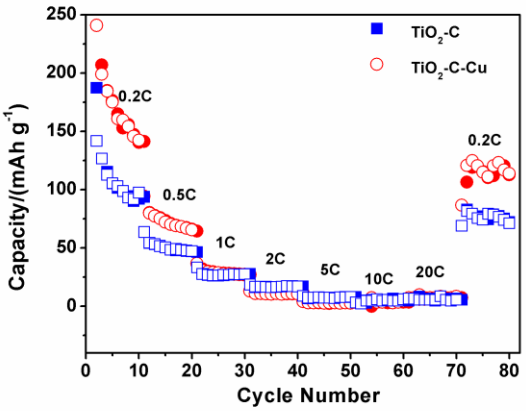

Figure 8. High rate discharge-charge performance at different current densities of 0.2, 0.5, 1, 2, 5, 10, 20, 0.2 C for TiO_2-C and TiO_2-C-Cu composites.

Fig. 9a shows the cycle voltammogram (CV) of TiO_2-C-Cu fresh electrode after 1, 3 and 10 cycles at a slow scan rate of 0.1 mV s^{-1} in the voltage range of 1.0-3.0 V. All three CV curves in Fig. 9a display a cathodic peak at 1.70 V and an anodic peak at 2.01 V, corresponding to the Li-ion insertion/extraction reaction in anatase TiO_2 of Eq. 1. Only very small intensity and location changes can be observed with increasing cycles, suggesting a good reversibility of TiO_2-C-Cu. The interval between two peaks is 0.31 V, smaller than that of TiO_2 nanocrystals (0.49 V) [32, 33]. As the peak separation is determined by the overpotential required for the redox process, the narrower the interval between two peaks, the easier the Li^+ insertion/extraction process. In addition, the ratio of anodic to

cathodic peak current, i_{pa} / i_{pc}, is about 1, which can further demonstrate the redox electrode process of TiO_2-C-Cu is relatively stable and reversible.

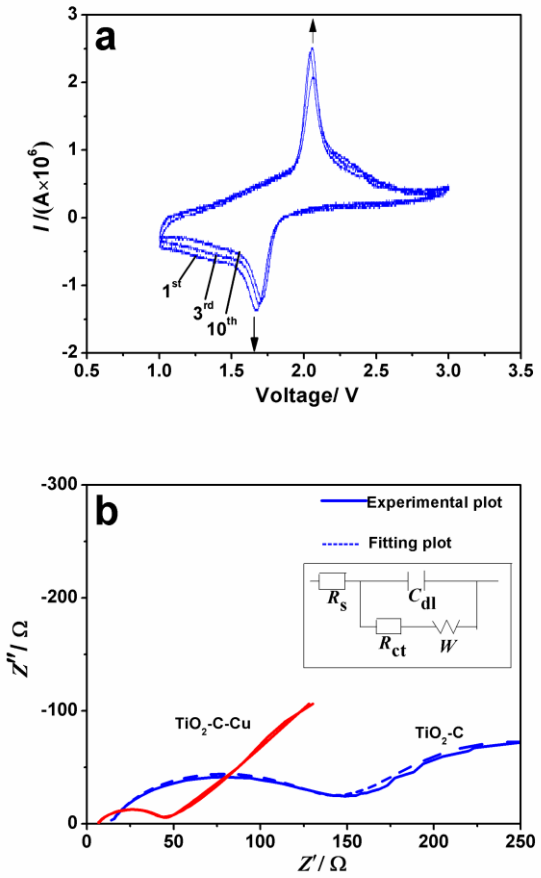

Figure 9. a Cycle voltammogram of TiO_2-C-Cu fresh electrode after 1, 3, 10 cycles at the scan rate of 0.1 mV s^{-1} (Voltage range: 1.0-3.0 V), and **b** Experimental points and fitting plots by the Nyquist-type plots for fresh TiO_2-C-Cu and TiO_2-C electrodes (Frequency range: 0.01 Hz – 100 kHz, Inset represents the equivalent circuit).

In order to estimate the kinetic parameters of the electrode process, we also carried out the electrochemical impedance tests. Fig. 9b shows the experimental and fitting curves of the Nyquist-type plots for the fresh electrodes of TiO_2-C-Cu and TiO_2-C, respectively. The equivalent circuit model, as shown in the inset in Fig. 9b, namely Randle model [34] was adopted, where R_S represents the bulk resistance of the electrolyte, separator and electrode; R_{ct} is related to the charge transfer resistance at the active material interface; Z_{dl} of constant phase element (CPE) represents the double-layer capacitance of the electrode–electrolyte interface; Warburg impedance, Z_W, is caused by a semi-infinite diffusion of Li^+ ion in electrode. Each parameter in the equivalent circuit was fitted by the Zview2 software. The fitting results of R_S and R_{ct} of TiO_2-C-Cu is 6.51 and 38.74 Ω, much smaller than 13.99 and 123.82 Ω of TiO_2-C, showing an obviously evidence of the electronic conductivity enhancement for TiO_2-C-Cu composite by "Cu-embedded". The exchange current density was further calculated by Eq. 2,

$$j_0 = RT / (nFR_{ct}) \quad (2)$$

where n = 1 for the transfer electron of Ti^{4+}/Ti^{3+} redox couple. The calculated values of the exchange current densities of TiO_2-C-Cu and TiO_2-C electrodes are 0.66 and 0.21 mA cm^{-2}, respectively.

The diffusion coefficient of Li^+ can be calculated through the Nyquist-type plots in the low-frequency region according to Eqs. 3 and 4:

$$D = 0.5 \cdot (RT)^2 / (n^2 A \sigma_W C F^2)^2 \quad (3)$$

$$Z' = R_s + R_{ct} + \sigma_W \omega^{-1/2} \quad (4)$$

where D is the diffusion coefficient, A is the contact area between electrode materials and electrolyte (here 0.50 cm^2), C is molar concentration of Li^+ (here 10^{-3} mol cm^{-3}), σ_W is the Warburg factor, Z' is the real resistance of the complex impedance plane and ω is the frequency. Plotting Z" against $\omega^{-1/2}$, σ_W can be obtained by the slope of the linear relationship of Eq. 4 in the low frequency range [35]. Then, the diffusion coefficient of lithium ion, D, in TiO_2-C-Cu and TiO_2-C were calculated to be around 4.56 10^{-10} and 9.87 10^{-11} cm^2 s^{-1}, respectively. As Maria et al. [36] reported that the diffusion coefficient of lithium ion for crystalline TiO_2 was about 10^{-13} cm^2 s^{-1}, and Wagemaker et al. [37] studied the diffusion coefficient of lithium ion in anatase films and found it was in the range of 10^{-10} - 10^{-17} cm^2 s^{-1}. Based on the reported values, the obtained values of lithium ion diffusion coefficient by the equivalent circuit are quite reasonable. The lithium ion diffusion coefficient in TiO_2-C-Cu is one order larger than that of TiO_2-C, and almost similar as that in single crystal, which provides further evidence of the superior behavior of TiO_2-C-Cu obtained by "Cu-embedded".

By increasing the electric conductivity as well as the lithium ion diffusion coefficient, "Cu-embedded" significantly enhances the high rate performance and the cycling stability of the composite electrode. So embedded-metal would play a much more significant role to improve the electrochemical properties when low-conductivity materials such as TiO_2 are used as the anode materials in lithium ion batteries.

4. CONCLUSIONS

Ordered Mesoporous TiO_2-C-Cu composites have been synthesized by mixing resol carbon precursor and $Cu(CH_3COO)_2$ *via* EISA method. The existence of carbon in the matrix effectively prevented the excessive growth of TiO_2 nanocrystals during the calcination. With the ordered mesoporous channels and a relative large surface area of 161.9 m^2 g^{-1}, TiO_2-C-Cu composites exhibited quite good high rate charge/discharge capacity as well as the cyclic stability. "Cu-embedded" significantly increased the electric conductivity and the diffusion coefficient of lithium ion, especially at low current density. Hence, "Cu-embedded" provided a much more facile and economic way to

enhance the electrochemical performance of low-conductivity crystalline TiO_2 as the anode material in lithium ion battery.

ACKNOWLEDGMENTS
This work was supported by the National Natural Science Foundation of China (No. 21176066), the 111 Project of Ministry of Education of China (No.B08021) and the Fundamental Research Funds for the Central Universities of China.

References

1. B. Scrosati and J. Garche, *J. Power Sources*, 195 (2010) 2419
2. Z. G. Yang, D. W. Choi, S. Kerisit, K. M. Rosso, D. H. Wang, J. Zhang, G. Graff and J. Liu, *J. Power Sources*, 192 (2009) 588
3. J. Wang, Y. Zhou, Y. Hu, R. O' Hayre and Z. Shao, *J. Phys. Chem. C*, 115 (2011) 2529
4. J. Li, Z. Tang and Z. Zhang, *Electrochem. Solid-State Lett.*, 8 (2005) A316
5. Y. Wang, M. Wu and W. F. Zhang, *Electrochim. Acta*, 53 (2008) 7863
6. P. Kubiak, J. Geserick, N. Husing and M. Wohlfahrt-Mehrens, *J. Power Sources*, 175 (2008) 510
7. H. Yamada, T. Yamato, I. Moriguchi and T. Kudo, *Solid State Ionics*, 175 (2004) 195
8. Z. Wang, S. Liu, G. Chen and D. Xia, *Electrochem. Solid-State Lett.*, 10 (2007) A77
9. D. Fattakhova-Rohlfing, M. Wark, T. Brezesinski, B. M. Smarsly and J. Rathousky, *Adv. Funct. Mater.*, 17 (2007) 123
10. L. Kavan, J. Rathousky, M. Gratzel, V. Shklover and A. Zukal, *Microporous Mesoporous Mater.*, 44–45 (2001) 653
11. D. Wang, D. Choi, Z. Yang, V. V. Viswanathan, Z. Nie, C. Wang, Y. Song, J. Zhang and J. Liu, *Chem. Mater.*, 20 (2008) 3435
12. M. Alvaro, C. Aprile, M. Benitez, E. Carbonell and H. Garcia, *J. Phys. Chem. B*, 110 (2006) 6661
13. M. C. Carbajo, E. Enciso and M. J. Torralvo, *Colloids Surf. A*, 293 (2007) 72
14. H. Shibata, T. Ogura, T. Mukai, T. Ohkubo, H. Sakai and M. Abe, *J. Am. Chem. Soc*., 127 (2005) 16396
15. D. H. Chen, F. Z. Huang, Y. B. Cheng and R. A. Caruso, *Adv. Mater.*, 21 (2009) 2206
16. E. L. Crepaldi, G. J. de A. A. Soler-Illia, D. Grosso, F. Cagnol, F. Ribot and C. Sanchez, *J. Am. Chem. Soc.*, 125 (2003) 9770
17. C. J. Brinker, Y. Lu, A. Sellinger and H. Fan, *Adv. Mater.*, 11 (1999) 579
18. B. Z. Tian, X. Y. Liu, B. Tu, C.Z. Yu, J. Fan, L. M. Wang, S. H. Xie, G. D. Stucky and D. Y. Zhao, *Nat. Mater.*, 2 (2003) 159
19. J. Tang, Y. Y. Wu, E. W. McFarland and G. D. Stucky, *Chem. Commun.*, (2004) 1670
20. R. L. Liu, Y. J. Ren, Y. F. Shi, F. Zhang, L. J. Zhang, B. Tu and D. Y. Zhao, *Chem. Mater.*, 20 (2008) 1140
21. J. W. Lee, M. C. Orilall, S. C. Warren, M. Kamperman, F. J. Disalvo and U. Wiesner, *Nat. Mater.*, 7 (2008) 222
22. Y. Ishii, Y. Kanamori, T. Kawashita, I. Mukhopadhyay and S. Kawasaki, *J. Phys. Chem. Solids*, 71 (2010) 511
23. Y. Zhou, Y. Kim, C. Jo, J. Lee, C. Lee and S. Yoon, *Chem. Commun.*, 47 (2011) 4944
24. Y. G. Guo, Y. S. Hu, W. Sigle and J. Maier, *Adv. Mater.*, 19 (2007) 2087
25. Y. Meng, D. Gu, F. Q. Zhang, Y. F. Shi, H. F. Yang, Z. Li, C. Z. Yu, B. Tu and D. Y. Zhao, *Angew. Chem. Int. Ed.*, 44 (2005) 7053
26. D. Y. Zhao, Q. S. Huo, J. L. Feng, B. F. Chmelka and G. D. Stucky, *J. Am. Chem. Soc.*, 120 (1998) 6024

27. J. L. Duan, J. Liu, D. Mo, H. J. Yao, K. Maaz, Y. Chen, Y. Sun, M. Hou, X. Qu, L. Zhang and Y. Chen, *Nanotechnol.*, 21 (2010) 365605
28. Y. Meng, D. Gu, F. Q. Zhang, Y. F. Shi, L. Cheng, D. Feng, Z. X. Wu, Z. X. Chen, Y. Wan, A. Stein and D. Y. Zhao, *Chem. Mater.*, 18 (2006) 4447
29. X. F. Qian, Y. Wan, Y. L. Wen, N. Q. Jia, H. X. Li and D. Y. Zhao, *J. Colloid Interface Sci.*, 328 (2008) 367
30. G. Nuspl, K. Yoshizawa and T. Yamabe, *J. Mater. Chem.*, 7 (1997) 2529
31. E. Baudrin, S. Cassaignon, M. Koesch, J. P. Jolivet, L. Dupont and J. M. Tarascon, *Electrochem. Commun.*, 9 (2007) 337
32. S. J. Bao, Q. L. Bao, C. M. Li and Z. L. Dong, *Electrochem. Commun.*, 9 (2007) 1233
33. T. Brezesinski, J. Wang, J. Polleux, B. Dunn and S. H. Tolbert, *J. Am. Chem. Soc.*, 131 (2009) 1802
34. S. B. Yang, X. L. Feng and K. Müllen, *Adv. Mater.*, 23 (2011) 3575
35. G. Q. Liu, L. Wen, G. Y. Liu, Q. Y. Wu, H. Z. Luo, B. Y. Ma and Y. W. Tian, *J. Alloys Compd.*, 509 (2011) 6427
36. L. S. Maria, M. R. Kevin and J. Liu, *J. Phys. Chem. C*, 114 (2010) 20277
37. M. Wagemaker, R. van de Krol, A. P. M. Kentgens, A. A. van Well and F. M. Mulder, *J. Am. Chem. Soc.*, 123 (2001) 11454